Proton and neutron alignments and transition strengths in the transitional nucleus ^{81}Rb

S. L. Tabor, P. D. Cottle, C. J. Gross,* U. J. Hüttmeier,† and E. F. Moore‡
Departmentof Physics, Florida State University, Tallahassee, Florida 32306

W. Nazarewicz
Institute of Physics, Warsaw Institute of Technology, PL-00662 Warsaw, Poland
and Supercomputer Computations Research Institute, Florida State University, Tallahassee, Florida 32306
(Received 9 November 1988)

High-spin states in ^{81}Rb were investigated with the ^{55}Mn(^{29}Si, $2pn$)^{81}Rb reaction using a 95.2 MeV ^{29}Si beam. γ-γ coincidences were measured with three detectors at 23° and ±100°. The yrast and near-yrast rotational bands in ^{81}Rb have been extended well above the first band crossings, with spin assignments based on the directional correlations of oriented nuclei. The mean lifetimes of many higher levels were measured using the Doppler shift attenuation method. They imply moderate deformations with average transition moments of 2–2.5 eb, except at the sharp band crossing in the negative parity band, where they dip by a factor of 2. The data have been analyzed in terms of the Woods-Saxon cranking model. The crossing observed in the positive-parity band is attributed to the alignment of a $g_{9/2}$ neutron pair. Two negative-parity bands observed above $I=\frac{15}{2}$ are suggested to contain $(g_{9/2})^2$ neutron and proton pairs, respectively.

I. INTRODUCTION

The shapes of the odd $A\approx 80$ nuclei can be strongly influenced by the unpaired nucleon (see, e.g., Refs. 1–4). If the configurations available to the unpaired nucleon are kept constant with a fixed odd number of nucleons, the effects of variations in the number of paired nucleons of opposite isospin can be investigated. The light Rb isotopes ($Z=37$) provide an excellent series to study. Much is known[5–12] about the rotational properties of the Rb isotopes with neutron numbers extending from near the middle of the f-p-g shell to near its closure at $N=50$. One expected[13] effect is a general increase in deformation as the nucleon numbers approach the middle of the shell at a particle number of 39.

The isotope ^{81}Rb occupies a crucial position at the middle of this sequence, but its rotational properties were not as well known as those of its lighter neighbors prior to the present work. In particular, the known negative-parity band ended in what appeared to be part of a strong backbend, and only three yrast transitions were known. The yrast band had not been investigated to high enough spins to determine whether a change occurs in its properties leading to reduced signature splitting and greatly increased $M1$ transition strengths. Such a change has been seen nearby in ^{81}Kr (Ref. 1), ^{81}Sr (Refs. 3 and 4), and ^{85}Rb (Ref. 10).

Previous work on ^{81}Rb includes measurements of the spins and parities of the ground and first excited metastable states using atomic beam magnetic resonance techniques.[14–16] Low-spin excited states were studied[17,18] following the β^+ decay of ^{81}Sr. The high-spin level scheme of ^{81}Rb has been investigated[6] up to spins of $\frac{21}{2}^+$ and $\frac{21}{2}^-$ with α and ^{16}O fusion-evaporation reactions. Some early lifetime measurements were made[5] in the yrast positive-parity band. A more complete set of measurements have been made[7] up to the $\frac{17}{2}^-$ and $\frac{21}{2}^+$ states.

The present investigation was undertaken to learn more about the structure of ^{81}Rb at high spin. γ-γ coincidences were measured at 23° and ±100° following the production of ^{81}Rb at high angular momentum in a heavy-ion fusion-evaporation reaction. The coincidence data provided information on the positions, spins and lifetimes of a number of new levels in ^{81}Rb. The results have been compared with Woods-Saxon Strutinsky-Bogolyubov cranking calculations.

II. EXPERIMENTAL PROCEDURE

High-spin states in ^{81}Rb were populated using the ^{55}Mn(^{29}Si,$2pn$)^{81}Rb reaction at a laboratory beam energy of 95.2 MeV. This reaction was chosen because ^{81}Rb is one of its strongest products, along with ^{81}Sr and ^{78}Kr. The ^{29}Si beam was obtained from its 4.7% abundance in natural Si. To avoid further loss of intensity, the ^{29}Si beam was stripped only once to a charge state of 8^+ and accelerated to an energy of 77.4 MeV in the FN tandem accelerator. The necessary additional acceleration was provided by the Florida State University superconducting linac. The target consisted of 2 mg/cm^2 of ^{55}Mn evaporated onto an 0.013 cm thick Pb backing which stopped the ^{81}Rb recoils as well as the beam.

The electromagnetic decay cascades were detected in three Ge detectors with relative efficiencies of about 25%. One Compton suppressed[19] Ge detector was placed at a forward angle of 23° and another at 100°. An unsuppressed Ge(Li) detector was placed at 100° on the other side of the beam. The energy signals from each coincident pair of detectors were digitized, monitored and written on magnetic tape. A ^{152}Eu source was used to determine the efficiency and initial energy calibrations. After the experiment internal energy calibrations were

determined by least squares fitting the energies of the following γ rays to linear functions of channel number: 74.3, 84.77, 87.3 (Pb x-rays), 175.6 (^{80}Rb), 188.3 (^{81}Rb from β^+ decay), 454.9, 664.2 (^{78}Kr), 511.0 (γ^{+-}), 1227.0 and 1524.61 keV (^{42}Ca). These calibrations were used to gain shift each channel number to a uniform dispersion of 1 keV per channel before sorting[20] into two two-dimensional arrays in the memory of a Ridge 3200 computer. The 100°–100° coincidences were histogrammed into a folded triangular array of 2500 channels on a side, while the 23°–100° coincidences were accumulated into a square array of 2500 by 2500 channels.

Coincidence spectra were obtained by projection from these two arrays. The 23° spectra projected from energy gates on the 100° axis of the square array were used to determine lifetimes using the Doppler-shift attenuation method (DSAM). The ratios of the γ ray intensities in these spectra to those in the 100° spectra projected from energy gates on the 23° axis of the square array were used to determine the directional correlation of oriented (DCO) nuclei ratios for spin assignments. Due to the construction of the triangular array, projection from a single energy gate produces a spectrum equal to the sum of the spectra in each 100° detector gated by the other one. The 100° spectra projected from the triangular array were added to the 100° spectra projected from 23° gates on the square array for use in constructing the level scheme.

III. CONSTRUCTION OF THE LEVEL SCHEME

The high-spin level scheme of ^{81}Rb inferred from the present as well as previous[5,6,17,18] work is shown first in Fig. 1 as a guide for the discussion. For simplicity only the yrast and near-yrast states are shown. A number of other nonyrast states were reported from β^+ decay studies[17,18] and many of them were also seen in the present work, but they are not involved in the decay sequences shown.

Information on the electromagnetic transitions observed in ^{81}Rb is also listed in Table I. All the energies listed were determined in the present work except for that of the lowest $\frac{7}{2}^+$ state, which was taken[17,18] to be 86.3 keV. They have been corrected for Doppler shifting by calculating the unshifted energy from the measured energies at 23° and 100°. The transition and level energies determine in the present work are very close to those observed in previous work.[5–7] A precise comparison cannot be made because the previous values were quoted to only the nearest keV, but the present values may be systematically lower by up to 1 keV. The analog to digital converters used in the present work are very linear, and the internal energy calibrations described in Sec. II yielded fits with average deviations of about 0.1 keV between 74 and 1525 keV.

The DCO ratios were determined from the 23°–100° coincidence intensities according to

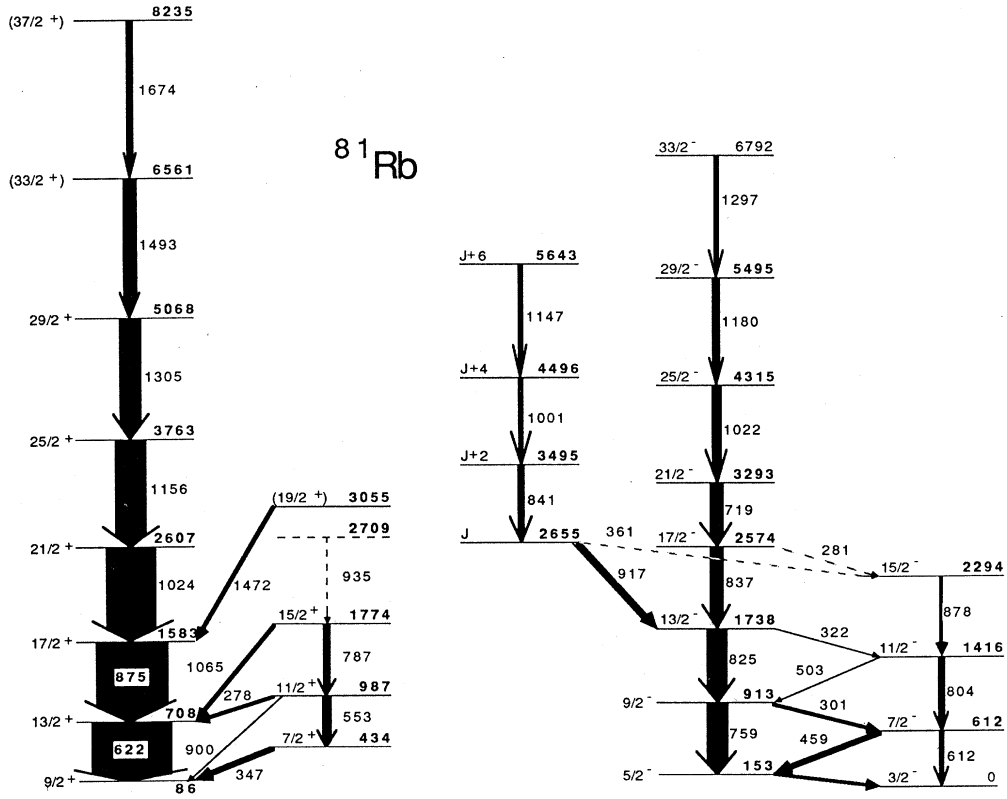

FIG. 1. The yrast and near-yrast level scheme of ^{81}Rb as deduced from the present and previous work. The widths of the arrows are approximately proportional to the intensities of the decay transitions.

$$R_{\mathrm{DCO}}=\frac{I(\gamma \text{ at } 23^\circ \text{ gated by } \gamma_G \text{ at } 100^\circ)}{I(\gamma \text{ at } 100^\circ \text{ gated by } \gamma_G \text{ at } 23^\circ)},$$

where the gating transition γ_G was always one or more of known $E2$ multipolarity. The DCO ratios are expected[4,21] to be about unity for unmixed $E2$ transitions and to vary from nearly 0 to 2 for $\Delta J=1$ transitions, depending on the multipole mixing ratio. Systematics show that most $M1/E2$ DCO ratios in these yrast cascades lie near or somewhat above $\frac{1}{2}$.

TABLE I. Properties of the electromagnetic transitions observed in ^{81}Rb. Uncertainties in the last digits are shown in parentheses.

E_i (keV)	E_γ (keV)	J_i^π	J_f^π	R_{DCO}
433.6	347.3	$\frac{7}{2}^+$	$\frac{9}{2}^+$	0.52(5)
708.6	622.3	$\frac{13}{2}^+$	$\frac{9}{2}^+$	1.24(4)
986.8	278.2	$\frac{11}{2}^+$	$\frac{13}{2}^+$	0.51(4)
986.8	553.2	$\frac{11}{2}^+$	$\frac{7}{2}^+$	1.34(10)
986.8	900.4	$\frac{11}{2}^+$	$\frac{9}{2}^+$	0.47(7)
1583.1	874.5	$\frac{17}{2}^+$	$\frac{13}{2}^+$	0.93(4)
1774.1	787.4	$\frac{15}{2}^+$	$\frac{11}{2}^+$	1.21(4)
1774.1	1065.5	$\frac{15}{2}^+$	$\frac{13}{2}^+$	
2606.8	1023.7	$\frac{21}{2}^+$	$\frac{17}{2}^+$	1.03(5)
2709	935		$\frac{15}{2}^+$	
3054.6	1471.5	$(\frac{19}{2}^+)$	$\frac{17}{2}^+$	0.45(7)
3763.0	1156.2	$\frac{25}{2}^+$	$\frac{21}{2}^+$	1.17(6)
4820	1057	$(\frac{27}{2}^+)$	$\frac{25}{2}^+$	0.52(10)
5068.1	1305.1	$\frac{29}{2}^+$	$\frac{25}{2}^+$	1.03(8)
6561	1493	$(\frac{33}{2}^+)$	$\frac{29}{2}^+$	0.75(10)
8235	1674	$(\frac{37}{2}^+)$	$(\frac{33}{2}^+)$	1.16(10)
153.1	153.1	$\frac{5}{2}^-$	$\frac{3}{2}^-$	0.72(4)
611.7	458.6	$\frac{7}{2}^-$	$\frac{5}{2}^-$	0.86(4)
611.7	611.8	$\frac{7}{2}^-$	$\frac{3}{2}^-$	1.05(10)
912.5	300.7	$\frac{9}{2}^-$	$\frac{7}{2}^-$	0.54(5)
912.5	759.4	$\frac{9}{2}^-$	$\frac{5}{2}^-$	1.07(4)
1415.5	503	$\frac{11}{2}^-$	$\frac{9}{2}^-$	
1415.5	803.8	$\frac{11}{2}^-$	$\frac{7}{2}^-$	
1737.7	322.2	$\frac{13}{2}^-$	$\frac{11}{2}^-$	0.64(8)
1737.7	825.2	$\frac{13}{2}^-$	$\frac{9}{2}^-$	0.99(4)
2293.6	878.1	$\frac{15}{2}^-$	$\frac{11}{2}^-$	1.10(10)
2574.3	281.5	$\frac{17}{2}^-$	$\frac{15}{2}^-$	
2574.3	836.6	$\frac{17}{2}^-$	$\frac{13}{2}^-$	0.97(5)
2654.7	917.0	J	$\frac{13}{2}^-$	0.81(8)
3293.4	719.1	$\frac{21}{2}^-$	$\frac{17}{2}^-$	0.98(5)
3495.3	840.6	$J+2$	J	0.96(6)
4315.3	1021.9	$\frac{25}{2}^-$	$\frac{21}{2}^-$	1.09(5)
4496	1001	$J+4$	$J+2$	1.00(10)
5495	1180	$\frac{29}{2}^-$	$\frac{25}{2}^-$	1.14(8)
5643	1147	$J+6$	$J+4$	1.06(10)
6792	1297	$\frac{33}{2}^-$	$\frac{29}{2}^-$	1.03(10)

A. Positive-parity bands

The yrast band in the odd mass 80 nuclei is usually built on a $g_{9/2}$ particle because of its large intrinsic spin. Due to its yrast nature, this band is usually populated the most strongly. The yrast band in ^{81}Rb is no exception. The $g_{9/2}$ band has previously[5,6] been identified up to $\frac{21}{2}^+$. Gates on these transitions show that much higher spin states were populated in the present reaction. The sum of the coincidence spectra gated on most of these transitions is shown in Fig. 2 as a composite view of the cascade. Most of the strong peaks have been assigned to the main cascade based on the individual coincidence spectra. The level ordering follows from the γ-ray intensities and effective lifetimes and is consistent with rotational systematics. The DCO ratios are generally close to unity and consistent with those of $\Delta J=2$, $E2$ transitions. This agrees with previous[5,6] $E2$ assignments for the lower transitions. The value of 0.75 for the DCO ratio of the 1493 keV γ ray could imply a $\Delta J=1$ transition, but is more likely to be due to the difficulty in recognizing all of the yield in the strongly Doppler-shifted and broadened 23° spectrum. We have used the rotational systematics to tentatively assign a $\Delta J=2$ multipolarity to this transition, but have placed the spin in parenthesis.

Many of the $g_{9/2}$ bands in this mass region exhibit strong signature splitting so that the states of unfavored signature ($\alpha=-\frac{1}{2}$) lie just below the $\alpha=+\frac{1}{2}$ states of the next higher spin. This signature splitting is even larger in ^{81}Rb, leading to a level inversion so that, e.g., the $\frac{11}{2}^+$ state lies above the $\frac{13}{2}^+$ one. A spin of $\frac{11}{2}^+$ was previously assigned to the 987 keV state on the basis of $\Delta J=1$ decays to the $\frac{9}{2}^+$ and $\frac{13}{2}^+$ states. Spins of $\frac{7}{2}^+$ and $\frac{15}{2}^+$ for the 434 and 1774 keV states, which were favored in previous work,[6] appear rather definite now. The measured multipolarities of the decay transitions are consistent with these spins and just these states are selectively populated in the heavy-ion high-spin reaction. The usual yrast arguments[22] imply that only the states which increase

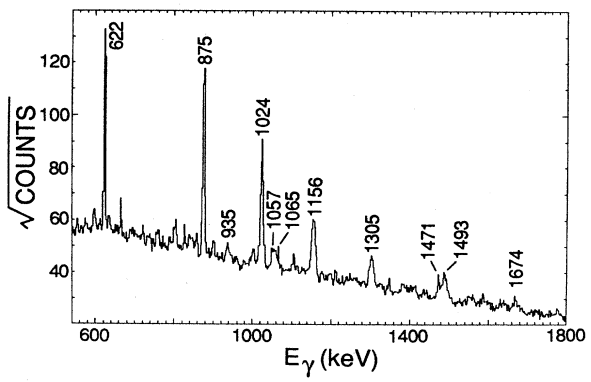

FIG. 2. The spectrum of γ rays at 100° in coincidence with the 622, 875, 1024, 1156, 1305, and 1493 keV transitions in the yrast positive-parity band. The square root of the number of counts is displayed along the ordinate to provide a moderate compression of the dynamic range and a constant height for the statistical fluctuations. The peaks are labeled by their energies in keV.

maximally in spin with excitation energy will be populated strongly.

Several additional γ rays are clearly seen in coincidence with positive parity transitions in ^{81}Rb. The narrow 1472 keV peak is in coincidence only with the 622 and 874 keV transitions and has a DCO ratio characteristic of a $\Delta J = 1$ transition. This places it in the level scheme at 3055 keV and implies a most likely spin of $\frac{19}{2}^+$. The coincidence relations of the weaker 935 keV transition imply that it most likely decays from a state at 2709 keV to the 1774 keV level. The state has been indicated with a dashed line in Fig. 1 because the limited statistical accuracy of the peak and the lack of other decay branches lend a small uncertainty to its exact placement. It was not possible to determine a reliable DCO ratio for the 935 keV transition. The 2709 and 3055 keV states are both candidates to be the fourth member of the $\alpha = -\frac{1}{2}$ band.

A Doppler broadened 1057 keV peak was seen in the 622, 874, 1024, and possibly the 1156 keV gates and these γ rays were seen in the 1057 keV gate. Hence, it represents a transition to either the $\frac{25}{2}^+$ or $\frac{21}{2}^+$ states. Because of this uncertainty, it has not been placed in the level scheme. Recent work by the Rossendorf group[23] may resolve this question. The DCO ratio implies a multipolarity change of $\Delta J = 1$ and a most likely spin of $\frac{27}{2}^+$ or $\frac{23}{2}^+$ depending on which is the final state.

B. Negative-parity bands

The lower-spin portion of the near-yrast negative-parity bands was also established in earlier work[6] and confirmed in the present study. The sum of the spectra in coincidence with the first four transitions in the favored $\alpha = +\frac{1}{2}$ band is shown in Fig. 3. A number of new peaks can be seen. The strongest ones at 1022, 1180, and 1297 keV are in coincidence with each other as well as with the first four transitions and appear to represent the continuation of the $\alpha = +\frac{1}{2}$ band. The DCO ratios for all three transitions imply $E2$ multipolarity, leading to the indicated spins. Several members of the $\alpha = -\frac{1}{2}$ band have also been seen, in confirmation of previous results. The 878 keV transition which was tentatively observed previously is clearly seen in the present work with a DCO ratio characteristic of an $E2$ transition. There is some evidence for a 281 keV γ ray feeding the 2294 keV state, but the statistics are not definitive.

There is also evidence in Fig. 3 for a sequence of peaks at 917, 1001, and 1147 keV. A careful inspection of the 837 keV peak in the 825 and 759 keV gates reveals a partially resolved peak on the high-energy side which does not appear in the 719 keV or higher gates. Fits to the sum of two Gaussian peaks indicate a rather consistent centroid of 840.6 keV for the higher, weaker peak. These four transitions are in coincidence with each other, as well as with the 759 and 825 keV decays. This is shown most clearly by the spectrum in Fig. 4 gated by the 917 keV transition. The short effective lifetimes of the 1001 and 1147 keV transitions place them at the top of the cascade in the order shown in Fig. 1, while the 841 and 917 keV decays show no Doppler shifting. The 917 keV γ ray has been placed below the 841 keV one because of its higher intensity in most of the gates. However, some variations in the shape of the 917 keV peak may indicate contaminants in that region which may increase its apparent strength. The DCO ratios for the 841, 1001, and 1147 keV lines imply that they are $E2$ transitions. The DCO ratio of 0.81 for the 917 keV γ ray may possibly indicate a $\Delta J = 1$ transition or more likely problems with the possible contaminant. The 361 keV transition to the $\frac{15}{2}^-$ state and yrast arguments that the observed states in-

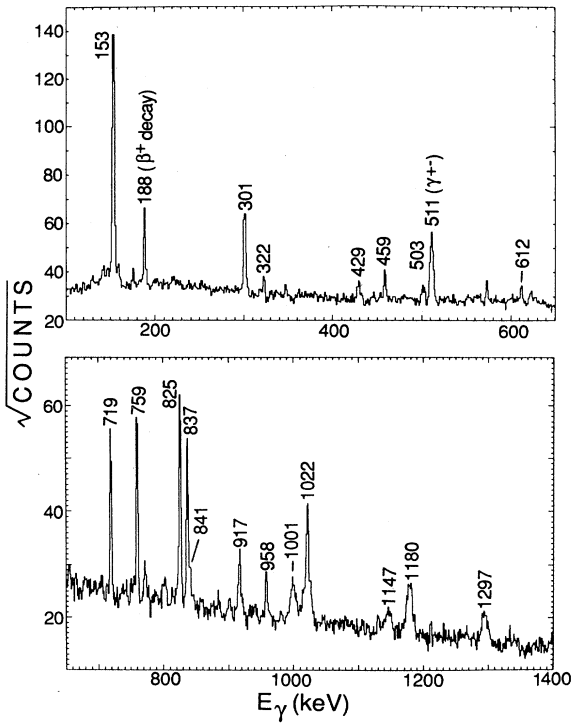

FIG. 3. The spectrum of γ rays at 100° in coincidence with the 759, 825, 837, and 719 keV transitions in the lowest negative-parity band. The square root of the number of counts is graphed along the ordinate.

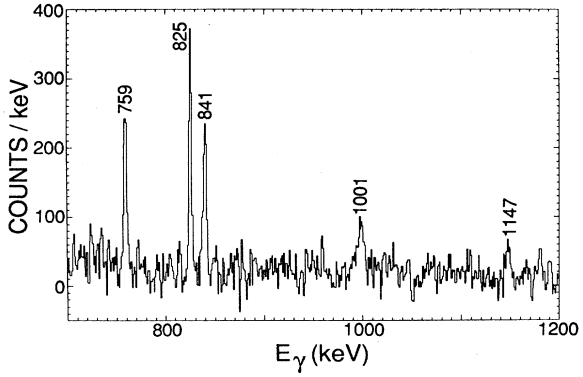

FIG. 4. The spectrum of γ rays at 100° in coincidence with the 917 keV transition.

crease maximally with spin make it most likely that $J^{\pi}=\frac{17}{2}^{-}$ for the 2655 keV level. However, the state has been labeled an unknown "J" in Fig. 1 because of the weakness of the 361 keV transition which appears in some gated spectra but not in others.

Several additional transitions have been seen but not indicated on the level scheme because of uncertainties in their placement. Two of these are visible in Fig. 3 at 429 and 958 keV. The third is another 301 keV γ ray in addition to the $\frac{9}{2}^{-}$ to $\frac{7}{2}^{-}$ decay. This γ ray is clearly seen in the 301, 759, and 804 keV gates, which should not be in coincidence with the $\frac{9}{2}^{-}$ to $\frac{7}{2}^{-}$ transition. The existence of two transitions with indistinguishable energies complicates the coincidence analysis, but it appears that the 301, 429, and 958 keV decays are in coincidence with each other and feed into the $\frac{13}{2}^{-}$ state. It is not possible to determine the level ordering from the intensity ratios because each of these γ rays is also in coincidence with other, stronger decay sequences.

IV. LIFETIME MEASUREMENTS

Mean lifetimes have been measured for many transitions in ^{81}Rb using the Doppler-shift attenuation method (DSAM). The measured line shapes at 23° were fitted to ones calculated by simulating the deceleration and decay process, as described in Ref. 4. To remove overlapping γ rays, the 23° spectra were measured in coincidence with specific energy gates in the 100° detectors. The spectra gated by all the transitions below the one of interest in the decay sequence were generally added to give the best possible statistical accuracy.

In the simulation of the deceleration process the tabulated values[24] of the electronic stopping powers were scaled[25] to the experimental[26] stopping powers for He. The Bohr ansatz[27] was used to calculate the nuclear component of the stopping powers and the Blaugrund approximation[28] was used for the angular straggling due to atomic collisions. The simulation included the effects of beam energy loss in the target, a Gaussian distribution of recoil velocities and the finite solid angle of the Ge detector.

The line shape simulation took into account both the delays due to the observed feeding pattern from known states above the one of interest and those due to the unobserved "side" feeding into each level. The line shape fitting process was started with the highest transition with adequate statistical accuracy. Since there is no information about the feeding delays above this transition, the lifetime which best fits its line shape is an upper limit. This limit provides an effective lifetime representing the feeding delay for the transition below it. All of the measured lifetimes and intensities were used in the calculation of the line shapes below them.

The lifetimes listed in Table II are based on the direct feeding delays discussed above and on side feeding times which start at 0.1 ps for the highest transition and increase by 0.03 ps per MeV of deexcitation. This assumption gave good fits to the lineshapes and has been used in several recent studies of similar reactions.[4,29–31] Examples of the fits for a variety of lifetimes are shown in Fig. 5. Two other side feeding patterns were tried. One of these involved using a side feeding time for each level equal to the effective lifetime of the level above it, as in a recent study[32] of ^{80}Sr. Some of the line shape fits using this prescription were better and some were worse. The resulting lifetimes were similar or somewhat shorter, but within the error limits in Table II.

The other side feeding prescription involved allowing both the lifetime of a state and its side feeding time to vary for the best fit. The fits were generally slightly better; for example, in the region between the stopped and fully shifted peaks in the 1024 keV line shape (Fig. 5).

TABLE II. Mean lifetimes, electromagnetic transition strengths, and transition quadrupole moments in ^{81}Rb. Uncertainties in the last digits are shown in parentheses or as super or subscripts.

E_i (keV)	E_γ (keV)	τ (ps) Present	τ (ps) previous[a]	Adopted	$B(E2)$ (e^2fm^4)[b]	Q_t (eb)
709	622		8.7(4)	8.7(4)	1010^{50}_{45}	1.90^{5}_{4}
1583	874	1.05(20)	1.25(10)	1.18(10)	1360^{130}_{110}	2.10^{10}_{8}
2607	1024	0.48(9)	0.60(20)[c]	0.48(9)	1510^{350}_{240}	2.16^{24}_{18}
3763	1156	0.24(5)		0.24(5)	1650^{440}_{290}	2.22^{28}_{20}
5068	1305	<0.26[c]		<0.26[c]	>830	>1.56
612	612		5.3(5)	5.3(5)	530^{80}_{40}	1.94^{14}_{11}
913	759		2.1(3)	2.1(3)	1030^{180}_{130}	2.20^{18}_{15}
1416	804		1.5(2)	1.5(2)	1430^{230}_{180}	2.38^{19}_{15}
1738	825		4.8(5)	4.8(5)	425^{50}_{40}	1.24^{7}_{6}
2574	837		2.0(4)[c]	2.0(4)[c]	1000^{250}_{170}	1.80^{21}_{16}
3293	719	2.3(10)		2.3(10)	1850^{1400}_{550}	2.39^{79}_{39}
4315	1022	0.36(7)		0.36(7)	2030^{500}_{330}	2.47^{28}_{21}
5495	1180	0.34(8)		0.34(8)	1050^{500}_{260}	1.76^{38}_{23}
6792	1297	<0.35[c]		<0.35[c]	>630	>1.36

[a]Reference 7.
[b] 1 Weisskopf single-particle unit equals 20.8 e^2fm^4.
[c]Effective lifetime not corrected for feeding.

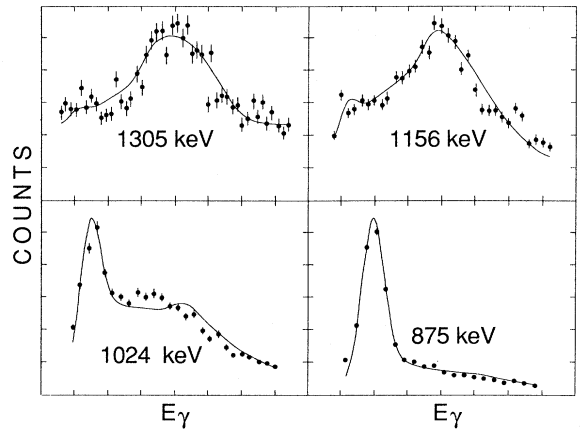

FIG. 5. The spectra of the 875, 1024, 1156, and 1305 keV γ rays at 23° in coincidence with all the transitions below them in the yrast decay sequence. The curves represent the results of calculations simulating the deceleration and emission process as described in the text.

The resulting lifetimes were close to those in Table II. With better statistical accuracy to more reliably determine two parameters for each lineshape, this technique would probably be the best.

The uncertainties in Table II reflect the uncertainties in side feeding times discussed above, as well as those in the stopping powers. Two previous measurements of lifetimes in ^{81}Rb have been reported. Only the more recent ones[7] are listed in Table II since they have superseded the older ones.[5] These measurements of the lower lying states overlap the present ones of higher states with shorter lifetimes in only two cases, where they agree within errors. It might appear that the present results are consistently shorter, but the previous value for the 2607 keV state is an effective lifetime and hence an upper limit.

It was not possible to obtain reliable line shape fits for the 1147 and 1001 keV transitions due to limited statistical accuracy and some contaminant lines. However, these γ rays exhibit considerable Doppler shifts which would imply lifetimes less than 1 ps. The absence of Doppler shifts for the 841 and 917 keV transitions imply lifetimes substantially greater than 1 ps.

V. TRANSITION FROM DEFORMED TO SPHERICAL SHAPES IN ODD-A Rb AND Y ISOTOPES

Both the deformed shell model theory and the experimental systematics predict the transition from a rotation to a vibrationlike pattern to take place around $N=44$ (see discussion in Ref. 33). The transitional nuclei around ^{82}Kr are γ and β soft and, therefore, are very sensitive to all the effects which are associated with shape variations. In odd-A nuclei one may expect very strong polarization effects coming from aligned quasiparticle excitations. In fact, such effects have been observed in many $N=43$ [^{79}Kr (Ref. 34), ^{81}Sr (Ref. 4), ^{83}Zr (Ref. 33)] and $N=45$ [^{81}Kr (Ref. 1)] isotones.

The decrease in collectivity when approaching $N=44$ is also clearly seen in the experimental data for odd-Z systems. The rubidium and yttrium isotopes are very good candidates for systematic study of this effect since the most neutron-deficient isotopes of Rb and Y known, ^{77}Rb (Ref. 8) and ^{81}Y (Ref. 35), are among the best collective rotors in the $A\approx 80$ mass region and their spectra, unlike those of the As and Br nuclei, are not strongly influenced by shape coexistence effects at low spins.

In Fig. 6 the positive parity levels[8–12,36] are compared for ^{77}Rb through ^{85}Rb, spanning a range of neutron numbers from $N=40$ near the middle of the shell to $N=48$ near the shell closure. The most consistent pattern seen is a steady increase in level energies, suggesting a decrease in deformation, as N increases toward the shell closure at $N=50$. Another experimental argument for the decrease in collectivity with neutron number comes from the measured lifetimes. The experimental $B(E2)$ values for the $\frac{13}{2}^+\rightarrow\frac{9}{2}^+$ transition are 2800(180), 2130(120), 1010(50), and 234(27) e^{2}fm^4 for ^{77}Rb (Ref. 8), ^{79}Rb (Refs. 36 and 37), ^{81}Rb, and ^{85}Rb (Ref. 10), respectively. The variation in deformation influences the Coriolis coupling. It can be seen in Fig. 6 that there is a substantial increase in signature splitting in the $g_{9/2}$ bands when going towards $N=50$. This effect can be directly associated with the transition from the strong coupling limit (characteristic of well-deformed systems) to weak coupling (characteristic of near-spherical nuclei). The transition takes place around $N=44$. For ^{77,79}Rb and ^{81}Y the lowest $\pi=+$ state has $I=\frac{5}{2}$ while for the heavier isotopes with $N\geq 42$ it is an $I=j=\frac{9}{2}$ state that becomes the band head of the $g_{9/2}$ band.

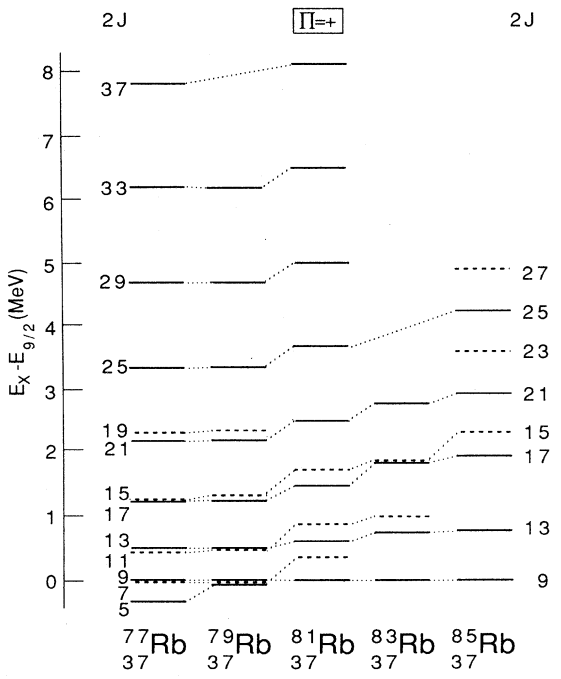

FIG. 6. The positive-parity yrast level schemes of the light Rb isotopes relative to the positions of the $\frac{9}{2}^+$ states. Solid (dashed) lines indicate states of signature $\alpha=+\frac{1}{2}$ ($\alpha=-\frac{1}{2}$).

The near-yrast negative-parity levels in $^{77-83}$Rb are compared in Fig. 7. The same trend of decreasing deformation with increasing N can be seen among the lower levels. The trend is not so clear above 2.5 MeV where the backbend occurs in ^{81}Rb. The signature splitting is rather small for ^{77}Rb and increases somewhat with N. No states of signature $\alpha=-\frac{1}{2}$ have been reported for ^{79}Rb.

Theoretically, the properties of ^{77}Rb can be well described in terms of a large prolate deformation,[38] while the experimental data for ^{85}Rb have been well understood by spherical shell model calculations[10] with ^{88}Sr as an inert core. The intermediate Rb isotopes have been analyzed by Coriolis coupling calculations (see e.g., Refs. 6, 36, and 39) after assuming a sizable triaxiality ($\gamma\approx-27°$, according to the Lund convention) and a gradual reduction of β_2 with increasing N. The single-proton band head calculations of Ref. 2 indeed suggest a very well deformed ($\beta_2\approx0.38$) configuration for ^{77}Rb and a deformation softness in ^{81}Rb (the calculated prolate-oblate energy difference for the $g_{9/2}$ configuration is only about 200 keV).

VI. CRANKING SHELL MODEL ANALYSIS OF EXPERIMENTAL DATA

A more detailed comparison can be made from a cranking model analysis of the level schemes and transition quadrupole moments Q_t. The dynamical moments of inertia $J^{(2)}$ and the Q_t values for the $\pi=+$ bands in ^{77,79,81}Rb and ^{81,83}Y are graphed as functions of the rotational frequency ω in Fig. 8. The values of $J^{(2)}$ and ω are derived, as usual, from the measured transition energies (assuming $K=\frac{3}{2}$), and the Q_t values, from the measured lifetimes. A broad upbend indicating a band crossing with strong interaction can be seen in the dynamical moments of inertia for ^{81}Rb and ^{83}Y at $\hbar\omega\approx0.55$ MeV. This effect decreases rapidly with decreasing neutron number.

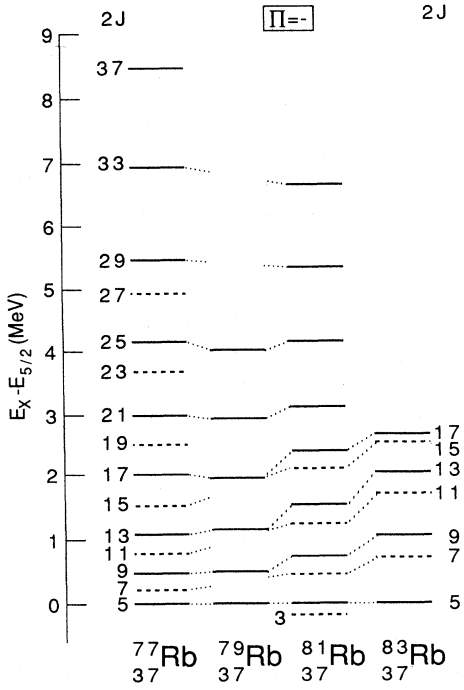

FIG. 7. The negative-parity near yrast level schemes of the light Rb isotopes relative to the positions of the $\frac{5}{2}^-$ states. States with signature $\alpha=+\frac{1}{2}$ ($-\frac{1}{2}$) are drawn with solid (dashed) lines.

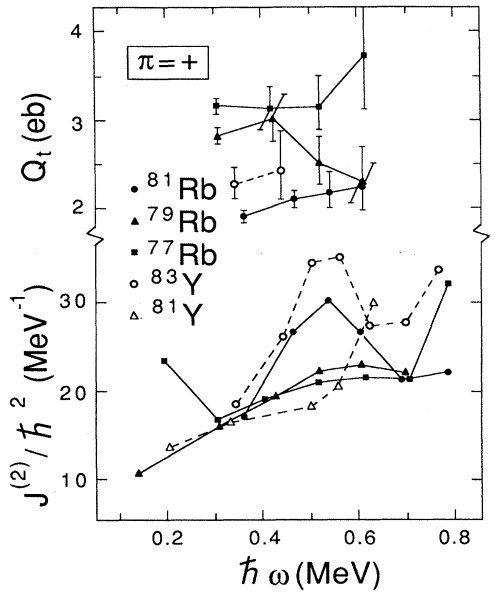

FIG. 8. The dynamical moments of inertia $J^{(2)}$ and the transition quadrupole moments Q_t as a function of rotational frequency ω for the $\pi=+$, $\alpha=+\frac{1}{2}$ states in ^{77,79,81}Rb and ^{81,83}Y.

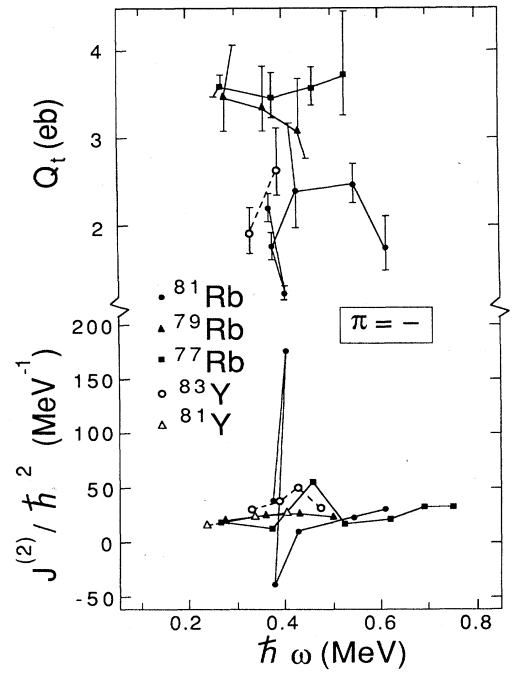

FIG. 9. The dynamical moments of inertia $J^{(2)}$ and transition quadrupole moments Q_t as a function of rotational frequency ω for the $\pi=-$, $\alpha=+\frac{1}{2}$ states in ^{77,79,81}Rb and ^{81,83}Y.

Another alignment may be starting in ^{77}Rb and ^{83}Y at $\hbar\omega > 0.7$ MeV.

The transition quadrupole moments confirm suggestions that ^{81}Rb and ^{83}Y are less deformed than the lighter isotopes. The Q_t values in ^{81}Rb do increase smoothly with spin—suggesting a stretching effect. On the other hand, those of ^{79}Rb fall considerably at the crossing region. ^{77}Rb maintains the highest level of deformation, with a value of Q_t consistently above 3 eb. It is interesting to observe that the Q_t values in ^{81}Rb are lower compared to those in ^{83}Y, suggesting that the latter nucleus is slightly more deformed.

The backbending in the lowest-negative-parity band in ^{81}Rb can be clearly seen in Fig. 9 as a sharp rise and fall in $J^{(2)}$ near the rotational frequency of 0.4 MeV. Note that the vertical scale for $J^{(2)}$ has been compressed considerably compared to that in Fig. 8 to show this large excursion. Such sharp backbends are rare in the $A \approx 80$ region. Note that there is a corresponding sharp dip in the quadrupole transition strengths in ^{81}Rb at $\hbar\omega \approx 0.4$ MeV, in agreement with a sharp band crossing picture. Even away from the dip, the Q_t values for ^{81}Rb are substantially lower than for ^{79}Rb or ^{77}Rb, as in the positive-parity bands. They show its reduced deformation more clearly than do the level spacings.

Experimental Routhians for ^{81}Rb and ^{83}Y are presented in Fig. 10 as functions of $\hbar\omega$. Our reference parameters $J_0 = 15\hbar^2/\text{MeV}$ and $J_1 = 4\hbar^4/\text{MeV}^3$ are the same as those chosen for ^{83}Zr in Ref. 33. The large signature splitting in the $g_{9/2}$ bands is clearly seen in Fig. 10. It is systematically larger by about 180 keV in ^{81}Rb as compared to ^{83}Y. This is consistent with larger deformation in ^{83}Y as discussed above. Another signature-dependent effect is the early upbending at around $\hbar\omega \approx 0.48$ MeV in the unfavored $(\alpha = -\frac{1}{2})g_{9/2}$ band in ^{83}Y which occurs at considerably lower frequency than in the favored band. Such a phenomenon is typical of a shape change associated with a band crossing.

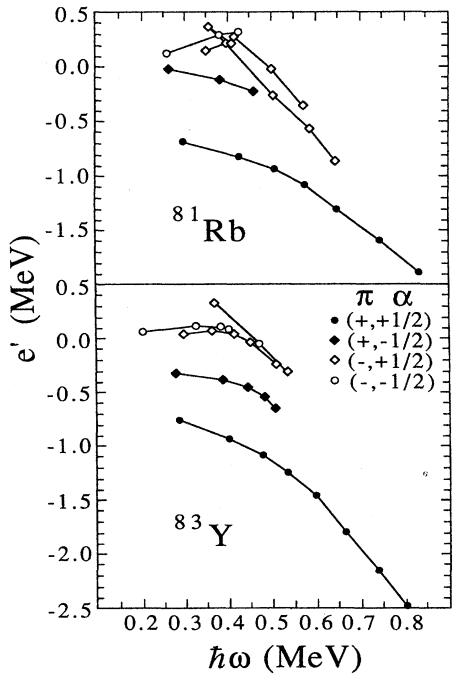

FIG. 10. Experimental Routhians for ^{81}Rb and ^{83}Y. The reference parameters are $J_0 = 15\,\hbar^2/\text{MeV}$, $J_1 = 4\,\hbar^4/\text{MeV}^3$.

The spin labeled "J" in Fig. 1 most likely has a value of $\frac{17}{2}$. If it were of $\frac{15}{2}$, then the second negative-parity band would lie about 600 keV higher in energy and, therefore, would probably be too weakly populated to be observed. This assignment implies that there are no $\alpha = -\frac{1}{2}$ negative-parity states observed above the band crossing. After the sharp band crossing at $\hbar\omega \approx 0.4$ MeV there is a fork in the $\pi = -$ sequence in ^{81}Rb. Both $\alpha = \frac{1}{2}$ bands carry very similar alignment which is about 1.5–2 $\hbar$ larger than that of the $g_{9/2}$ favored band.

A very interesting phenomenon observed in the odd-A nuclei around ^{82}Sr is the presence of 3-qp strongly coupled bands connected by $M1$ transitions. They have been seen above the first $g_{9/2}$ band crossing in ^{79}Kr (Ref. 34), ^{81}Kr (Ref. 1), and ^{81}Sr (Refs. 4 and 40), and explained in terms of an oblate to prolate deformation change induced by the aligned $g_{9/2}$ protons. In the odd-Z neighbors a similar $\Delta I = 1$ sequence has been observed in ^{85}Rb above the $I^\pi = \frac{21}{2}^+$ state (see Fig. 6) and in the negative-parity band[41] in ^{83}Y (above $I^\pi = \frac{17}{2}^-$). It has been speculated[41] that this $\Delta I = 1$ band in odd-Z nuclei contains two aligned $g_{9/2}$ neutrons. In ^{83}Y this band becomes nearly degenerate with the $\pi = -$ yrast band at the highest spins; see Fig. 10. We looked for the analogous structure in ^{81}Rb but there is no evidence for its presence in our data.

VII. THEORETICAL ANALYSIS

A theoretical analysis of the high-spin properties of ^{81}Rb has been carried out using the Woods-Saxon model of Ref. 2. The pairing force was assumed to be of the monopole type and the rotation was treated by means of the cranking approximation. In all details the procedure used in this paper follows the method described in Refs. 4 and 33 where more details and additional references can be found.

A. The positive-parity states

The calculated total Routhian surfaces (TRS) in the (β_2, γ) plane for the favored $(\alpha = \frac{1}{2})$ $g_{9/2}$ configuration in ^{81}Rb are shown in Fig. 11. At each (β_2, γ) grid point the total Routhian was minimized with respect to the hexadecapole deformation, β_4. At low rotational frequencies the TRS are very soft with respect to γ deformation, and the absolute minimum at $\hbar\omega = 0.29$ MeV corresponds to the triaxial near-prolate shape with $\beta_2 \approx 0.29$, $\gamma \approx -11°$. A quasiparticle diagram representative of the favored one-quasiparticle (1-qp) $g_{9/2}$ configuration is shown in Fig. 12. At this deformation the first crossing corresponds to the alignment of $g_{9/2}$ protons at $\hbar\omega_p \approx 0.53$ MeV, but it is blocked in the positive-parity band. The frequency of the neutron crossing is slightly higher,

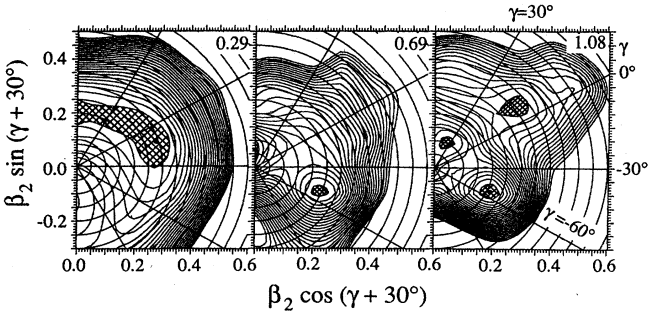

FIG. 11. Total Routhian surfaces (with pairing) in the (β_2,γ) plane for the $(\pi=+,\ \alpha=\frac{1}{2})$ configuration in ^{81}Rb. The numbers give values of rotational frequency (in MeV). The distance between contour lines is 200 keV and the circles of constant β_2 are spaced 0.05 apart.

$\hbar\omega_n \approx 0.65$ MeV, and the band interaction is larger. This would lead to a more gradual alignment of the $g_{9/2}$ neutrons. The next proton crossing (a BC crossing) is predicted at an even higher frequency, $\hbar\omega > 0.8$ MeV at this deformation point. The calculated minimum for the unfavored $(\alpha=-\frac{1}{2})$ $g_{9/2}$ band (not shown in Fig. 11) can be associated with positive γ deformation: $\beta_2 \approx 0.29$, $\gamma \approx 13°$. At this shape the pattern of the lowest neutron excitations resembles that of Fig. 12, and the same is true for the lowest proton Routhians—there is only a small shift (around 30 keV) towards lower frequencies.

The second TRS presented in Fig. 11, $\hbar\omega=0.69$ MeV, corresponds to the situation after the first band crossing. The minimum is moved toward the oblate axis and the quadrupole deformation β_2 is reduced. At this near-oblate shape, $\beta_2 \approx 0.24$, $\gamma \approx -50°$, the neutron crossing occurs at a much lower frequency, $\hbar\omega_n \approx 0.42$ MeV, but the proton BC crossing is delayed even more (see Fig. 13). Such a deformation change is characteristic of the situation when the aligning particles (here: neutrons) occupy the upper half of a high-j (here: $g_{9/2}$) subshell.

The bump in $J^{(2)}$ observed at $\hbar\omega \approx 0.52$ MeV (see Fig. 8) can, therefore, be associated with the neutron $g_{9/2}$ alignment inducing a shape change from the near-prolate to the near-oblate region. Because of the strong variation of ω_n with γ it is impossible to predict the exact value of the neutron crossing frequency on the basis of the quasiparticle diagrams shown in Figs. 12 and 13. A reasonable estimate of ω_n would be the average value extracted from Fig. 12 (for the 1-qp band) and Fig. 13 (for the 3-qp band), i.e., $\frac{1}{2}$ (0.65+0.42) MeV=0.54 MeV, in a fair agreement with experimental data. Our calculations do not support the suggestion of Ref. 41 about the proton character of the crossing in the $g_{9/2}$ band in ^{83}Y. The BC crossing frequency is predicted to occur at $\hbar\omega \approx 0.8$ MeV which is far too high, even after taking into account the uncertainty of the model.

At still higher frequencies the near-oblate minimum is stabilized, see the TRS at $\hbar\omega=1.08$ MeV in Fig. 11. This prediction also holds for the unfavored $\pi g_{9/2}(\nu g_{9/2})^2$ band. It is interesting to note that the signature splitting in the 3-qp band is expected to be reduced after the neutron crossing (cf., Figs. 12 and 13). Experimentally, however, no candidates for the unfavored 3-qp sequence have been observed in ^{81}Rb to confirm this prediction. On the

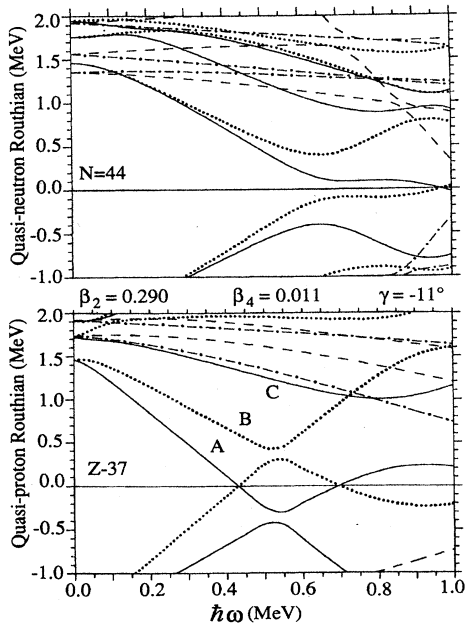

FIG. 12. Quasiparticle Routhians for ^{81}Rb at a deformation of $\beta_2=0.29$, $\gamma=-11°$, $\beta_4=-0.011$, characteristic of the one-quasiparticle $g_{9/2}$ bands. The spin and parity of Routhians are indicated in the following way: $(+,\frac{1}{2})$, full line; $(+,-\frac{1}{2})$, dotted line; $(-,\frac{1}{2})$, dot-dashed line; $(-,-\frac{1}{2})$, dashed line. The pairing gap and the Fermi level were fixed at the values corresponding to $\omega=0$. The conventional labels (A,B,C) are indicated for the Routhians discussed in the text.

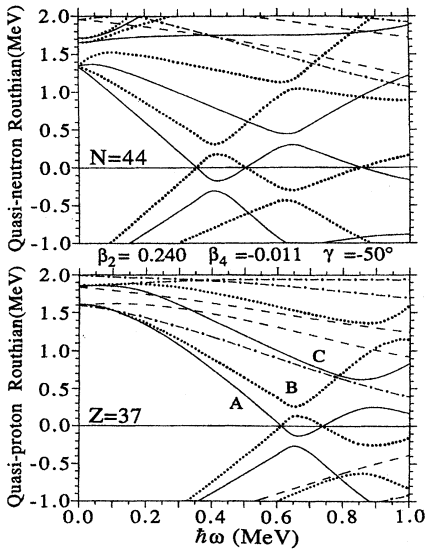

FIG. 13. Similar to Fig. 12, but at a deformation of $\beta_2=0.24$, $\gamma=-50°$, $\beta_4=-0.011$, typical of the three-quasiparticle bands involving a $\nu g_{9/2}$ pair.

other hand, the last experimental points for ^{83}Y shown in Fig. 10 suggest that such an effect indeed takes place.

B. The negative-parity states

The lowest-negative-parity 1-qp excitations in ^{81}Rb can be well understood in terms of $f_{5/2}-p_{1/2}$ mixing. A strong Coriolis mixing at low spins leading to the reduction of $B(E2)$ values around the $K=\frac{3}{2}$ band head was suggested by the asymmetric-rotor-plus-particle model[7] (a similar quenching of the quadrupole strength at low spins has also been observed[41] in the $\pi=-$ band in ^{83}Y). In these calculations, however, a significant triaxiality ($\gamma\approx-26°$) has been assumed in order to reproduce the observed signature splitting and electromagnetic rates.

The calculated TRS for the lowest ($\pi=-$, $\alpha=-\frac{1}{2}$) configuration in ^{81}Rb are shown in Fig. 14. At low frequencies, $\hbar\omega=0.29$ MeV, the total nuclear potential is very γ soft, and very shallow near-prolate and near-oblate local minima can be seen. This probably would explain why the assumption of an effective triaxiality in Ref. 7 was successful. Experimentally, the lowest $\pi=-$ Routhian has signature $\alpha=\frac{1}{2}$. This is consistent with the results presented in Figs. 12 and 13 and confirms a dominating role for the $f_{5/2}$ ([301]$\frac{3}{2}$,[303]$\frac{5}{2}$) and $p_{1/2}$ ([301]3/2) subshells in building the negative-parity band.

Unlike the case of the $g_{9/2}$ band, the first proton crossing is not blocked here. The aligned quasiprotons are expected to polarize the core towards near-prolate shapes while the neutron Routhians would trigger a shape change towards $\gamma=-60°$. This is illustrated in the second TRS in Fig. 14 for $\hbar\omega=0.59$ MeV. At the near-oblate minimum ($\gamma=-55°$) there are two $g_{9/2}$ neutrons aligned and no $g_{9/2}$ protons. The near-prolate configuration cannot, unfortunately, be easily separated because the low-lying noncollective oblate ($\gamma=60°$) state disturbs the picture (such a separation would be possible after going to the energy-versus-spin representation). We have checked, however, that in the deformation region of $\beta_2\approx0.15$, $\gamma>0°$ the corresponding quasiparticle vacuum contains two aligned $g_{9/2}$ protons and no aligned $g_{9/2}$ neutrons.

The picture of the two competing S bands, based on the proton and the neutron excitations, is typical of Kr and Sr nuclei with $N>46$ [see e.g., Ref. 42 where

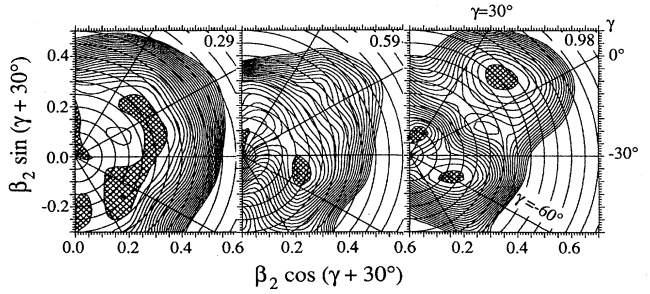

FIG. 14. Similar to Fig. 11, but for the ($\pi=-$, $\alpha=-\frac{1}{2}$) configuration in ^{81}Rb. The ($\pi=-$, $\alpha=+\frac{1}{2}$) TRS are very similar.

($\pi g_{9/2}$)^2 and ($\nu g_{9/2}$)^2 bands have been found in ^{82}Kr]. The relative position of the neutron and proton $g_{9/2}$ bands changes rapidly with the number of particles. For example, g-factor measurements have assigned the S band in ^{84}Sr to the neutron configuration,[43] while the proton structure for the S band in ^{82}Sr has been suggested by another recent study.[44] A very similar situation has also been found in the transitional nuclei around ^{128}Ba where the competing $\nu h_{11/2}$ and $\pi h_{11/2}$ configurations lie very close in energy, see e.g., Ref. 45. In both regions, i.e., $A\approx80$ and $A\approx128$, the aligned neutrons drive the system towards near-oblate shapes while the protons polarize the core towards near-prolate shapes. As a consequence, the standard additivity rules of the cranking shell model cannot directly be applied and additional experimental information is needed (such as the g factor measurements quoted above) before it can be definitely concluded which of the two aligned bands is the neutron or the proton S band, respectively.

In view of above it is very difficult to make a definite statement which of the two observed 3-qp negative-parity bands in ^{81}Rb contains the $g_{9/2}$ proton-neutron pair. Our calculations speak in favor of the neutron excitation, but the aligned proton structure is very close in energy. The conclusion of Ref. 46 about the proton band crossing is based on the additivity properties of quasiparticle excitations and, therefore, should be taken with some caution.

The last diagram in Fig. 14 shows TRS at $\hbar\omega=0.98$ MeV, representative of the 5-qp configuration, containing two aligned $g_{9/2}$ protons and two aligned $g_{9/2}$ neutrons. The 5-qp band is expected to have an oblate shape ($\beta_2\approx0.18$, $\gamma\approx-60°$). A pronounced well deformed minimum ($\beta_2\approx0.46$) is also seen. The corresponding configuration contains two $h_{11/2}$ neutrons (for more details about this well deformed band we refer the reader to Refs. 4, 33, and 38).

Let us finally comment on the very low value of the crossing frequency in the $\pi=-$ band. Such a dramatic even-odd staggering in ω_p has already been observed in a number of nuclei from the $A\approx80$ mass region (see e.g., Refs. 31 and 46). It can be explained in terms of the reduced pairing in the negative parity configurations (note that in the quasiparticle diagrams shown in Figs. 12 and 13 the pairing gaps were kept fixed at values corresponding to zero rotational frequency), or by shape changes in the crossing region (see discussion in Sec. VII A).

VIII. SUMMARY

The present investigation of the structure of ^{81}Rb at high angular momentum has confirmed previous work and extended the lowest positive- and negative-parity rotational bands well beyond the first band crossings. Additional levels have been located, including a cascade of four transitions which feeds into the $\frac{13}{2}^-$ state. DCO ratios were measured for most of the transitions to help determine their multipolarities. The mean lifetimes of many of the higher transitions have been measured using the DSAM by fitting the forward-angle lineshapes.

This investigation has confirmed that the yrast and near-yrast structure of ^{81}Rb is generally consistent with

the other odd Rb isotopes with $N<50$. There is no dramatic reduction in signature splitting and shift to $\Delta J=1$ transitions in the positive parity band as has been seen in ^{81}Kr, ^{81}Sr, and ^{85}Rb. There is, however, a steady increase in collectivity as the neutron number decreases from the shell closure at $N=50$. ^{81}Rb occupies an intermediate position in this sequence and the transition quadrupole moments clearly show that it is less deformed than its lighter neighbors.

In one way ^{81}Rb deviates substantially from this intermediate position among the light Rb isotopes. It shows the strongest band crossing effects among the states of both parities. This is particularly true of the sharp backbend in the negative parity band, which is accompanied by a substantial drop in the transition moments.

A theoretical analysis was performed using the Woods-Saxon cranking model. A gradual alignment in the $g_{9/2}$ band can be explained in terms of the $g_{9/2}$ neutron crossing associated with a shape transition towards near-oblate shapes. The fork observed in the negative-parity band above $I=\frac{13}{2}$ is, most likely, caused by an independent alignment of the $g_{9/2}$ neutron and the $g_{9/2}$ proton pairs. Our calculations suggest that the neutron band is lower in energy, but this conclusion depends very much on the correct value of the prolate-oblate energy difference which is computed with an accuracy of a few hundred keV. Clearly, some additional experiments are needed (e.g., g factor measurements) to answer the question of which one of these two bands is lower. At still higher angular momenta the proton and neutron bands are expected to be crossed by a five-quasiparticle structure $\pi(f_{5/2}+p_{1/2})\otimes(\pi g_{9/2})^2\otimes(\nu g_{9/2})^2$.

ACKNOWLEDGMENTS

The work of J. D. Fox, A. D. Frawley, E. G. Myers, L. Wright, P. Allen, and all the other persons involved in the construction of the Florida State University superconducting linac is gratefully acknowledged. We would like to thank L. Funke for discussing recent results of his group on ^{81}Rb. This work was supported in part by the U.S. National Science Foundation. One of us (W.N.) was also supported by the Florida State University Supercomputer Computations Research Institute which is partially funded by the U.S. Department of Energy through Contract No. DE-FC05-85ER250000, and by the Polish Ministry of Science and Higher Education through Contract CPBP 01.09.

*Present address: Zweites Physikalisches Institut der Universität Göttingen, Bunsenstrasse 7-9, D-3400 Göttingen, Federal Republic of Germany.

†Present address: Department of Physics, University of Pennsylvania, Philadelphia, PA 19104.

‡Present address: Physics Division, Argonne National Laboratory, Argonne, IL 60439.

[1]L. Funke, F. Dönau, J. Döring, P. Kemnitz, E. Will, G. Winter, L. Hildingsson, A. Johnson, and Th. Lindblad, Phys. Lett. **120B**, 301 (1983).

[2]W. Nazarewicz, J. Dudek, R. Bengtsson, T. Bengtsson, and I. Ragnarsson, Nucl. Phys. **A345**, 397 (1985).

[3]E. F. Moore, P. D. Cottle, C. J. Gross, D. M. Headly, U. J. Hüttmeier, S. L. Tabor, and W. Nazarewicz, Phys. Rev. C **38**, 696 (1988).

[4]E. F. Moore, P. D. Cottle, C. J. Gross, D. M. Headly, U. J. Hüttmeier, S. L. Tabor, and W. Nazarewicz, Phys. Lett. **211B**, 14 (1988).

[5]H.-G. Friederichs, A. Gelberg, B. Heits, K. P. Lieb, M. Uhrmacher, K. O. Zell, and P. von Brentano, Phys. Rev. Lett. **34**, 745 (1975).

[6]H.-G. Friederichs, A. Gelberg, B. Heits, K. O. Zell, and P. von Brentano, Phys. Rev. C **13**, 2247 (1976).

[7]J. Panqueva, H. P. Hellmeister, L. Lühmann, K. P. Lieb, F. J. Bergmeister, P. von Brentano, and R. Richter, Nucl. Phys. **A376**, 367 (1982).

[8]L. Lühmann, K. P. Lieb, C. J. Lister, B. J. Varley, J. W. Olness, and H. G. Price, Europhys. Lett. **1**, 623 (1986).

[9]C. J. Lister, B. J. Varley, D. E. Alburger, P. E. Haustein, S. K. Saha, J. W. Olness, H. G. Price, and A. D. Irving, Phys. Rev. C **28**, 2127 (1983).

[10]L. Lühmann, K. P. Lieb, A. Moussavi-Zarandi, J. Panqueva, and J. Sau, Z. Phys. A **313**, 297 (1983).

[11]K. P. Lieb, L. Lühmann and B. Wörmann, in *Nuclei Off the Line of Stability*, ACS Symposium Series No. 324, edited by Richard A. Meyer and Daeg S. Brenner (American Chemical Society, New York, 1986).

[12]W. Gast, K. Dey, A. Gelberg, U. Kaup, F. Paar, R. Richter, K. O. Zell, and P. von Brentano, Phys. Rev. C **22**, 469 (1980).

[13]S. L. Tabor, Phys. Rev. C **34**, 311 (1986).

[14]J. P. Hobson, J. C. Hubbs, W. A. Nierenberg, H. B. Silsbee, and R. J. Sunderland, Phys. Rev. **104**, 101 (1956).

[15]J. C. Hubbs, W. A. Nierenberg, H. A. Shugart, and H. B. Silsbee, Phys. Rev. **104**, 757 (1956).

[16]J. C. Hubbs, W. A. Nierenberg, H. A. Shugart, H. B. Silsbee, and R. J. Sunderland, Phys. Rev. **107**, 723 (1957).

[17]R. Broda, A. Z. Hrynkiewicz, J. Styczen, and W. Walus, Nucl. Phys. **A216**, 493 (1973).

[18]T. A. Doron and M. Blann, Nucl. Phys. **A161**, 12 (1971).

[19]S. L. Tabor, Nucl. Instrum. Methods **B24/25**, 1031 (1987).

[20]S. L. Tabor, Nucl. Instrum. Methods **A265**, 495 (1988).

[21]K. S. Krane, R. M. Steffen, and R. M. Wheeler, Nucl. Data Tables **11**, 354 (1973).

[22]E. K. Warburton, J. W. Olness, C. J. Lister, R. W. Zurmühle, and J. A. Becker, Phys. Rev. C **31**, 1184 (1985).

[23]L. Funke (private communication).

[24]L. C. Northcliffe and R. F. Schilling, Nucl. Data Tables **A7**, 233 (1970).

[25]D. Ward, J. S. Forster, H. R. Andrews, I. U. Mitchell, G. C. Ball, W. G. Davies, and G. J. Costa, Atomic Energy of Canada Limited, Report No. AECL-5313 (1976) (unpublished).

[26]J. F. Ziegler and W. K. Chu, At. Data and Nucl. Data Tables **13**, 463 (1974).

[27]S. Kalbitzer, H. Oetzmann, H. Grahmann, and A. Feverstein, Z. Phys. A **278**, 223 (1976).

[28]A. E. Blaugrund, Nucl. Phys. **88**, 501 (1966).

[29]L. Funke, J. Döring, P. Kemnitz, E. Will, G. Winter, A. Johnson, L. Hildingsson, and Th. Lindblad, Nucl. Phys.

A455, 206 (1986).
[30]J. Heese, K. P. Lieb, L. Lühmann, F. Raether, B. Wörmann, D. Albor, H. Grawe, J. Eberth, and T. Mylaeus, Z. Phys. A **325**, 45 (1986).
[31]L. Lühmann, M. Debray, K. P. Lieb, W. Nazarewicz, B. Wörmann, J. Eberth, and T. Heck, Phys. Rev. C **31**, 828 (1985).
[32]R. F. Davie, D. Sinclair, S. S. L. Ooi, N. Poffe, A. E. Smith, H. G. Price, C. J. Lister, B. J. Varley, and I. F. Wright, Nucl. Phys. **A463**, 683 (1987).
[33]U. J. Hüttmeier, C. J. Gross, D. M. Headly, E. F. Moore, S. L. Tabor, T. M. Cormier, P. M. Swertka, and W. Nazarewicz, Phys. Rev. C **37**, 118 (1988).
[34]G. Winter, J. Döring, L. Funke, H. Prade, H. Rotter, R. Schwengner, A. Johnson, and A. Nilsson, J. Phys. G **14**, L13 (1988).
[35]C. J. Lister, R. Moscrop, B. J. Varley, H. G. Price, E.K. Warburton, J. W. Olness, and J. A. Becker, J. Phys. G **11**, 969 (1985).
[36]J. Panqueva, H. P. Hellmeister, L. Lühmann, F. J. Bergmeister, K. P. Lieb, and T. Otsuka, Nucl. Phys. **A389**, 424 (1982).
[37]J. Panqueva, H. P. Hellmeister, F. J. Bergmeister, and K. P. Lieb, Phys. Lett. **98B**, 248 (1981).
[38]W. Nazarewicz and T. Werner, in *Nuclear Structure of the Zirconium Region,* edited by J. Eberth, R. A. Mayer, and K. Sistemich (Springer-Verlag, Berlin, 1988).
[39]H. Toki and A. Faessler, Phys. Lett. **63B**, 121 (1976).
[40]G. C. Hicks, C. J. Gross, U. J. Hüttmeier, Xi-Ting Lu, G. Neuschaefer, and S. L. Tabor, Phys. Rev. C **29**, 1345 (1984).
[41]C. J. Lister, B. J. Varley, W. Fieber, J. Heese, K. P. Lieb, E. K. Warburton, and J. W. Olness, Z. Phys. A **329**, 413 (1988).
[42]P. Kemnitz, P. Ojeda, J. Döring, L. Funke, L. K. Kostov, H. Rotter, E. Will, and G. Winter, Nucl. Phys. **A425**, 493 (1984).
[43]C. Broude, E. Dafni, A. Gelberg, M. B. Goldberg, G. Goldring, M. Haas, O. C. Kistner, and A. Zemel, Phys. Lett. **105B**, 119 (1981).
[44]A. I. Kucharska, J. Billowes, and C. J. Lister (to be published); J. Billowes, (private communication), 1988.
[45]R. A. Wyss, A. Johnson, J. Nyberg, R. Bengtsson and W. Nazarewicz, Z. Phys. A **329**, 255 (1988).
[46]L. Funke, J. Döring, F. Dubbers, P. Kemnitz, E. Will, G. Winter, V. G. Kiptilu, M. F. Kudojarov, I. Kh. Lember, A. A. Pasternak, A. S. Mishin, L. Hildingsson, A. Johnson, and Th. Lindblad, Nucl. Phys. **A355**, 228 (1981).